Disintegration mechanisms of charged aqueous nanodroplets studied by simulations and analytical models

Kengo Ichiki and Styliani Consta*
Department of Chemistry, University of Western Ontario, London, Ontario, Canada N6A 5B7
(Dated: June 15, 2006)

The mechanism of fragmentation processes in aqueous nanodroplets charged with ions is studied by molecular dynamics (MD) simulations. Using constant-temperature MD, the evaporation of the water is naturally taken into account and sequences of ion fragmentation events are observed. The size of the critical radius of the charged droplet just before the fragmentation and the distribution of the sizes of the fragments are estimated. Comparison of the Rayleigh critical radius for fragmentation and simulation data is within 0.23 nm. This seemingly small difference arises from a large difference in the number of water molecules that makes fragmentation an activated process as in the ion evaporation mechanism (IEM). This finding is in agreement with the predictions of Labowsky *et al.* [*Anal. Chim. Acta* **2000**, *406*, 105–118] for charged aqueous drops. The size of the daughter droplets is larger than the prediction of Born's theory by 0.1 to 0.15 nm. The nature and the dynamics of the intermediate states of the fragmentation process characterized by a bridge formed between the mother droplet and the evaporating ion or thorned structures where the ion sits on the tip are important for the outcome of the size-distribution of the fragments, while it is missing in Born's theory.

Keywords: Electrospray, ion fragmentation, molecular dynamics, Rayleigh limit, ion evaporation mechanism.

I. INTRODUCTION

Fragmentation of liquid droplets charged with ions of the same sign is a process that has been studied for approximately one and a half centuries because of its fundamental and practical implications in aerosol chemistry. Questions that arise in fragmentation are about the number of charges that a droplet can hold just before it fragments, the possible fragmentation mechanisms and fragmentation channels before and after the Coulomb explosion limit. The stability of charged droplets has been addressed since the second half of the 19th century by Lord Rayleigh who gave a stability condition for a charged sphere subjected to small perturbations of its spherical shape.[1] In the last decades fragmentation of charged droplets has obtained particular practical significance because it is basic in electrospray mass spectrometry (ESMS).[2–5] Experiments in the field of ESMS have initiated the development of analytical models that capture the nature of the fragmentation mechanism.[6,7]

In electrospray there are two experimentally suggested fragmentation mechanisms, the charged residue mechanism (CRM)[6] and the ion evaporation mechanism (IEM).[7] In the former, ions are generated by successive instabilities as described by the Rayleigh theory, while in the latter, ion evaporation is treated as an activated process that follows first-order reaction kinetics. The CRM and IEM models have been extensively discussed in the literature and there is much controversy and debate regarding the extent to which each of the fragmentation mechanisms hold.[8–10] Discussions seem to be converging into an agreement that IEM holds for small ions, while CRM becomes the predominant mechanism for larger ions such as charged globular proteins. However, exceptions have been reported and the range of validity of each model is not yet well understood.[11] Even though there are analytical theories and experiments, molecular simulations of the fragmentation of charged clusters are very limited. Numerical study is quite important here because we can observe the fragmentation event directly. Whereas, traditional experimental techniques are unable to clearly observe the fragmentation event because of the nanoscale dimension of the clusters and the nanosecond time scale and thus prevent any clear understanding of the underlying mechanism.

The only known efforts of simulation studies of fragmentation of clusters initially prepared below Rayleigh's instability limit are Refs. 12–15. Coulomb explosion of metal clusters beyond Rayleigh's instability limit and at Rayleigh limit have been theoretically studied by Jortner and co-workers.[16–18] In Refs. 12,13 one of the authors of the present paper treated fragmentation as an activated process for droplets in which the ratio of ions to solvent molecules is such that the system is (meta)stable for several tens of nanoseconds. The fragmentation event was observed to occur through rare fluctuations in cluster shape, where a solvated ion leaves the droplet. The simulations were performed in an ensemble of constant temperature and number of molecules. On one hand, in those studies the temperature of the system was kept at 250 K so that the solvent evaporation events do not interfere with ion fragmentation, thus maintaining an ensemble with constant number of molecules. On the other hand, the effect of solvent evaporation was taken into account by studying a number of system sizes with constant number of ions and variable number of water molecules. The study introduces a new reaction coordinate (RC) that allows for the computation of the reversible work

(free energy) of the process along the RC and the estimation of the full rate constant. The key point in the calculation is that the RC associates the positions of all the ions and solvent molecules and in the way is constructed it can resolve fine details in the morphology of the clusters. Therefore, this RC can distinguish bottlenecked configurations that correspond to the barrier top of the free energy of the fragmentation. In those simulations a free energy barrier is found at the point of detachment of the solvated ion from the mother droplet. The question whether there is a 'late' transition state[4] as in IEM models has not been yet investigated with this simulation method.

In the present paper we follow a different approach: direct MD simulations are performed for a variety of sizes of systems that are much larger than those studied in Refs. 12,13. The goal is to understand which fragmentation mechanism may hold for various sizes of clusters and at varying temperatures. In the present simulations constant-temperature MD is used. The drawback of this method is that the time scale of the simulations becomes artificial. However, we can survey the ion-fragmentation for a wide range of droplet sizes, observing a sequence of fragmentation events from the initial conditions of the simulation to the final state, where most of the solvent molecules have been evaporated and the gas-phase ion is generated. Actually, in ESMS, a counter flow of dry gas is introduced to maintain the solvent evaporation. Without the supporting gas, the ions are covered by ice with an unknown number of water molecules and these extra water molecules prevent the mass measurement of the target residue. Therefore, the constant-temperature MD may be a valid simple description of the real systems.

The critical radius of the droplets just before fragmentation is compared with Rayleigh's model, while the size of the daughter droplets with Born's theory. It is found that even though the agreement in the critical radius between Rayleigh's model and simulations is within 0.23 nm, the nanodrops do not break down spontaneously through oblate-prolate fluctuations of increasing amplitude, but rather by sequential dissociation of single ion clusters from a parent multicharged cluster (except for the case that the number of ions is equal to two). The present data in combination with the findings in Refs. 12,13 indicate a dominant ion-evaporation type of mechanism. Actually, the dissociation of a solvated ion for charged aqueous nanodrops following the ion-evaporation mechanism has been also predicted to occur near the Rayleigh limit by the extended ion-evaporation model discussed in Ref. 19. One of the main findings of the simulations is that the intermediate states of the fragmentation process characterized by a bridge formed between the mother droplet and the evaporating ion or thorned structures where the ion sits on the tip are important for the outcome of the size-distribution of the fragments, while it is missing in Born's theory. Even though, some analytical theories estimate the shapes of intermediate states of macroscopic drops[19,20] microscopic details are important in nanodrops since the bottle-necks or thorns at the breaking point as well as the detached solvated ion are small systems where only several tens of solvent molecules participate in their formation. The significance of analyzing the configurations near the point of detachment has been brought up in Ref. 19 since this point determines the size of generated droplets and, therefore affects the ion-drop interaction following detachment. This point is particularly important for IEM models that consider a 'late' transition state. Finally, an extended ion-evaporation model[19] is tested to find the activation energy from the simulation data.

The outline of the paper is as follows: In Sec. II, the model system and simulation methods are described. In Sec. III, we analyze the numerical results on the sizes of daughter and main droplets and we compare with analytical theories. The conclusions of this study are presented in Sec. IV.

II. MOLECULAR DYNAMICS SIMULATIONS

A. Model and simulation method

In this paper, we study aqueous droplets negatively charged with chloride. The SPC/E model[21] is used for the water molecules and the force field developed by Chandrasekhar *et al.*[22] is used for the chlorine ions.[23] For the molecular dynamics engine, the GROMACS simulation software (version 3.2.1)[24] is used. The integration of Newton's equations of motion is performed by the leap-flog Verlet algorithm[25] with a time step of 1 fs. All simulations are done without periodic boundary conditions, and the translational and angular motions about the center of mass are removed at every step.

Initial configurations with various numbers of water molecules and ions are prepared in the following way: a bulk water configuration of 256 water molecules with periodic conditions is generated. A spherical region that contains $N + z$ water molecules is extracted out of the bulk configuration and z random sites of water molecules are replaced by ions. The potential energy of this initial configuration with N water molecules and z chloride ions is minimized by the low-memory Broyden-Fletcher-Goldfarb-Shannon scheme (implemented in GROMACS as "l-bfgs") with a force tolerance of at least 100 kJ/mol nm. Following the energy minimization, an equilibration run is executed for 100 ps or more at a temperature 250 K, at which the solvent evaporation is suppressed. Repeating this equilibrating run, we select independent initial configurations with the same parameters of N and z. The initial number of water molecules N is up to 1600 and that of ions z up to 11.

Following the preparation of initial conditions, we execute long time realizations until most solvent molecules have been evaporated. The temperature is kept constant by the Berendsen thermostat[26] or Nosé-Hoover thermostat[27,28] with a relaxation time of 0.1 ps. The

range of the temperature is between 350 and 450 K. A molecule is characterized as evaporated when the distance from the center of mass of the bulk of the droplet becomes larger than 10 nm, which is more than 4 times larger than the droplet radius. The system is checked for evaporating molecules every 1 ps and they are excluded from the simulation.

We have confirmed for several test cases that the results obtained with the above parameters hold for a smaller time step of 0.2 fs as well as for the thermostat relaxation time in the range 0.05 to 0.5 ps.

B. Stability of droplets

In each run of the constant temperature MD simulations, the general pattern found is that (1) a droplet shrinks as the water molecules depart from the droplet, (2) once the droplet reaches a particular size, characteristic of the given system, a single ion with several water molecules is emitted, (3) after the fragmentation, the main droplet has fewer charges in a smaller volume and becomes stable until the next fragmentation occurs. These observations match the experimental descriptions.[4] In a fragmentation process there are possible fragments of various sizes, therefore, we define an atom to belong to a fragment by the criterion that the atom-atom distance in that fragment is less than 1 nm. The largest fragment is called the *main* droplet and the smaller droplets containing ions are called the *daughter* droplets.

z	$T = 350$ [K]	370 [K]	400 [K]	450 [K]
2	42.3 ± 5.0 (6)	43.7 ± 3.9 (3)	54.3 ± 7.9 (4)	60.0 ± 10 (4)
3	98.2 ± 2.8 (5)	97.3 ± 5.8 (3)	112 ± 7.4 (3)	143 ± 22 (3)
4	177 ± 21 (6)	198 ± 16 (2)	210 ± 14 (3)	242 ± 25 (2)
5	297 ± 12 (5)	317 ± 53 (3)	314 ± 20 (3)	399 ± 82 (3)
6	415 ± 15 (5)	432 ± 12 (3)	457 ± 39 (3)	524 ± 93 (3)
7	589 ± 73 (5)	606 ± 29 (3)	600 ± 44 (3)	626 (1)
8	745 ± 130 (5)	830 ± 33 (3)	860 ± 59 (3)	852 ± 31 (3)
9	926 ± 56 (4)	1090 ± 45 (3)	1150 ± 98 (2)	1110 ± 7.1 (3)
10	1170 ± 49 (3)	1330 ± 73 (3)	1310 ± 37 (3)	1380 ± 69 (3)
11	1480 ± 31 (2)	1430 ± 24 (3)	1470 ± 30 (3)	1510 ± 23 (3)

TABLE I: Averages with the standard deviations of $N^*(z,T)$ from simulations. The numbers in parentheses are the number of fragmentation events at (z,T) collected in MD runs. To clarify the meaning of this number the following example is given: (2) at $(z,T) = (11, 350K)$ comes from two realizations with different initial configurations with $z = 11$ and $N = 1600$ while at $(z,T) = (10, 350K)$, (3) comes from two fragmentation events found in the two sequences of fragmentations starting from $z = 11$ and $N = 1600$ at $T = 350$K, and one event by starting from an initial configuration with $z = 10$ and $N = 1371$. In total 17 realizations were executed and 133 fragmentation events were collected.

In Table I, the critical size N^*, which is the number of water molecules at the fragmentation event, are summarized for realizations that we analyze in this article. Here, we define the moment of fragmentation by the time just before the charge of the main droplet decreases. Out of all realizations, there were only two fragmentation products observed: either a single ion with several solvent molecules or two ions with several solvent molecules. The former is more dominant product, while the latter is a much less frequent event. Two-ion fragmentation was observed only 6 times out of a total of 133 fragmentations.

The first question to address in the present MD simulations is whether the solvent evaporation affects the N^* where ion fragmentation occurs. To answer this question, let us examine simulations starting with $N = 1600$ and only two ions $z = 2$ at $T = 400$K and $T = 450$K. These droplets are quite stable over a long time period and ion evaporation is not observed until the number of water molecules becomes much smaller due to the solvent evaporation. It is interesting to note that the critical sizes N^* for these droplets with $z = 2$ are almost the same with N^* for $z = 2$ of the corresponding droplets starting with $N = 1600$ and $z = 11$. This shows that the critical sizes N^* are hardly affected by the history of solvent evaporation when the evaporation and fragmentation rates are slow, but are well determined by z and T.

III. COMPARISON BETWEEN SIMULATIONS AND ANALYTICAL MODELS

A. Measurement of Droplet Size

To compare with analytical theories the radius of the droplet R is a more relevant parameter than the number of solvent molecules N. The estimate of the radius of a cluster is approximate because of the roughness of the surface and the deviations from the spherical shape. Here we borrow methods used in the studies of protein folding and macromolecular docking, where the geometrical characterization is important. In these studies the following three surface models are widely used: the solvent accessible (SA) surface, the molecular surface (MS) and the van der Waals (VDW) surface.[29] The surface area and volume of those models have been calculated analytically[30,31] and the algorithms have been implemented in the program called "spacefill" in the molecular modeling software TINKER.[32] We calculate the radius of the corresponding sphere from the volume V of each model by $R = (3V/4\pi)^{1/3}$. The various models were tested and the results are presented in Appendix A. We select the SA model with subtraction of the probe radius defined by

$$R = \left(\frac{3V}{4\pi}\right)^{1/3} - R_p. \tag{1}$$

where V is the volume of the SA model and R_p is the probe radius, which is taken to be equal to 0.14 nm.

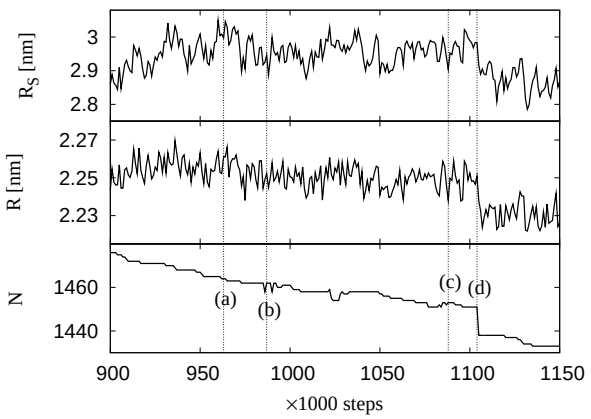

FIG. 1: Variations of the radius R_S estimated by the surface area (upper panel), R by the volume in Eq. (1) (middle panel), and N (lower panel) around the first fragmentation event in a simulation at $T = 350$ K. The marked configurations (a)-(d) correspond to the snapshots given in Fig. 2.

The reason that the volume V is used to estimate the radius of the cluster rather than the surface area S is that the latter fluctuates much more than the former. Typical sequences of fluctuations in the radius, determined by $R_S = (S/4\pi)^{1/2} - R_p$ and R by Eq. (1), around the fragmentation event are presented in the upper and middle panels of Fig. 1 with N in the lower panel. Besides the fluctuation difference between R_S and R, we also find that the values of the radii are quite different. This difference can be attributed to the roughness of the surface as well as the non-spherical shapes, which participate more in the estimation of the surface than the volume.

Snapshots of clusters that correspond to characteristic points marked (a)-(d) in Fig. 1 are shown in Fig. 2. Water molecules often form a thorn structure similar to a solar flare on the surface of the cluster. The thorns may consist only of water molecules, or they may sometimes include an ion. In Fig. 2 (a), thorns without an ion can be seen in the left- and right-top regions of the droplet, while a thorn with an ion is evident in the bottom region of the droplet. The thorn with an ion does not disintegrate in this occasion and the ion returns to the main droplet as shown in (b). In (c), there are two thorns with ions. After several tens of picoseconds (in the canonical dynamics) one of the thorns breaks down and a daughter droplet containing an ion and 13 water molecules departs from the main droplet as shown in (d). By visual inspection it was observed that the fluctuations that involve thorn structures are more frequent for charged systems than neutral systems. We define the *critical* radius $R^*(z)$ as the minimum radius of the droplet holding z ions. Since the droplet is evaporating, the radius is monotonically decreasing on average. Thus, approximately, the radius at the time of fragmentation corresponds to the critical radius. Even though V fluctuates less than S, it still does so to a considerable amount. Therefore, instead of taking the instantaneous value of V at fragmentation, we estimate the volume by applying a linear least-squares fitting on V for each segment between the fragmentations. This is an estimation of V at fragmentation with a constant decay rate of V in time (due to the solvent evaporation) for the segment where the number of ions in the droplet z is constant. From this volume, we finally obtain the critical radius $R^*(z)$ by Eq. (1). The size of the daughter droplets R_d is found by the instantaneous value of the molecular volume just after the fragmentation event.

B. Rayleigh Theory

Lord Rayleigh argued the influence of shape instability on the fragmentation of a charged droplet.[1] From the linear stability analysis for the spherical shape, it is found that the first unstable mode is the oblate-prolate oscillation. This analysis yields the famous relation for the critical radius as

$$R_R(z) = \left(\frac{e^2 z^2}{64\pi^2 \epsilon_0 \gamma} \right)^{1/3}, \tag{2}$$

where e is the elementary charge, ϵ_0 is the permittivity of vacuum, γ is the surface tension of the solvent.

a. Surface Tension To compare Rayleigh's theory with the simulations, the value of surface tension has to be imported in Eq. (2). Because of the lack of information on the surface tension of charged nanodroplets, the temperature dependence on γ is estimated from $\gamma(T) = B(1-T/T_c)^{\mu}\{1+b(1-T/T_c)\}$, where $B = 0.2358$ [N/m], $T_c = 647.096$ [K], $b = -0.625$ and $\mu = 1.256$, given for the bulk water by the International Association for the Properties of Water and Steam.[33] This choice facilitates the calibration of the results in this paper when the *correct* surface tension for the charged small droplet is available. Also, this would be acceptable to a certain accuracy especially for simulations of finite sized systems where there are large fluctuations, and therefore, larger statistical errors relative to bulk systems. The contribution into γ from a combination of both curvature and charge effects is not available for finite-sized systems. However, there are studies for simpler situations and these arguments we will employ here. The curvature effect (R-dependence) for pure liquids has been studied theoretically.[34] The first order correction is given by $\gamma = \gamma_0 (1 - 2\delta/R)$, where γ_0 is the bulk surface tension, δ is the Tolman length, and R is the radius of the droplet. Molecular dynamics simulations for water droplets show that at lower temperature, far from the critical point as in the present case, $\delta \approx 0.16\sigma$, where σ is the molecular diameter.[35] This means that the curvature correction to the bulk value is up to 10% even for a droplet with a radius of 1 nm.

The correction on γ due to the ions, even for bulk surfaces, is the most difficult to estimate. To our knowledge there are no studies on the surface tension of a charged droplet. As well, the specific ion effects on surface tension is still actively studied.[36,37] We may try to estimate

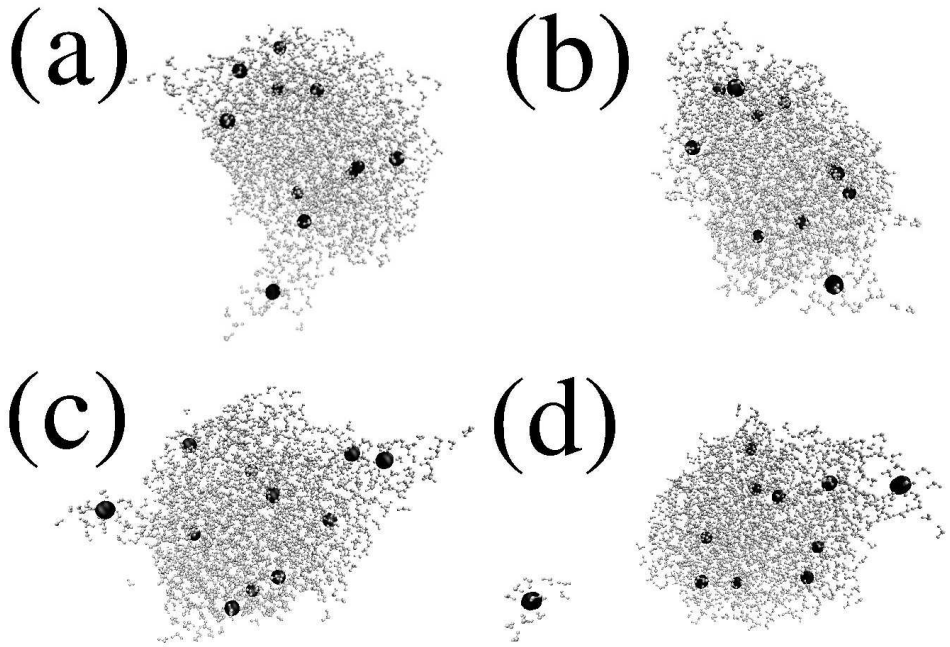

FIG. 2: Sequence of typical snapshots from the simulation presented in Fig. 1. The black spheres represent the Cl^- with the van der Waals radius. The oxygen and hydrogen sites of the water molecules are drawn by light gray spheres with 1/4 of the van der Waals radius. The size of the Cl^- is enlarged relative to the water molecules for visualization purposes.

the change of γ from the pure solvent case using the experimentally measured rate of surface tension change, $\mathrm{d}(\Delta\gamma)/\mathrm{d}c$, with concentration, c, for electrolytes in bulk solution. Here, $\Delta\gamma = \gamma(c) - \gamma(c = 0)$. This rate depends on the type of the electrolyte and it varies from -2.12 to 5.91 [mN m^{-1} / mol L^{-1}] for simple inorganic electrolytes.[38] The ion concentration in the simulations is up to 1.0 mol L^{-1}, so that the correction due to the presence of ions would be at most 8 % of the value with $c = 0$. Using the effect of the ions on γ for charged nanodroplets may not be unrealistic, due to the fact that in a bulk solution of electrolytes the flat surface has excess ions. The accumulation of the curvature and charge effects will lead to $\pm 10\%$ uncertainty on the value of surface tension for the charged nanodroplets relative to the value of a flat bulk surface of pure water.

b. Results In Fig. 3, the simulation data and Rayleigh's predictions are shown. In first view there is an apparent agreement of the critical radius within 0.23 nm between Rayleigh's predictions and simulation findings. The fragmentations found in simulations occur at $R^* > R_R$. Estimates of the charge ratio,

$$\frac{q}{q_R} = \left(\frac{e^2}{64\pi^2\epsilon_0\gamma}\right)^{1/2} \frac{z}{R^{*3/2}}, \qquad (3)$$

where q is the charge of the simulated droplet and q_R is the Rayleigh prediction, show that the fragmentation occurs on average at $87 \pm 3\%$ of q_R. Experimental measurements in the literature find similar behavior, where the ratio to the Rayleigh charge falls in the range between 60% to 104% for droplets with diameters from 4 to 200 micrometers with various solvents (methanol, water, heptane).[39] For nanodrops, Gamero-Castaño and Fernández de la Mora[40] reported a charge ratio from 57% to 72% for formamide droplets with tetraheptylammonium bromide and diameters between 2 and 5 nm. The good agreement between Rayleigh's predictions and simulations may lead to a first thought that a Rayleigh type micro-explosion that differs from the classical Rayleigh theory because of the discreetness of the model and the distribution of charge is the fragmentation mechanism. However, the arguments that follow indicate a dominant ion-evaporation type of mechanism.

If we take Rayleigh's condition as the "correct" energetic condition, then the seemingly small difference between R^* and R_R may arise by tens to hundreds of water molecules difference in the main droplet. As found in simulations (Table I) the range of variation of N^* in the main droplet, is from about 10 molecules in droplets that contain 2 to 3 single charges to a hundred of molecules

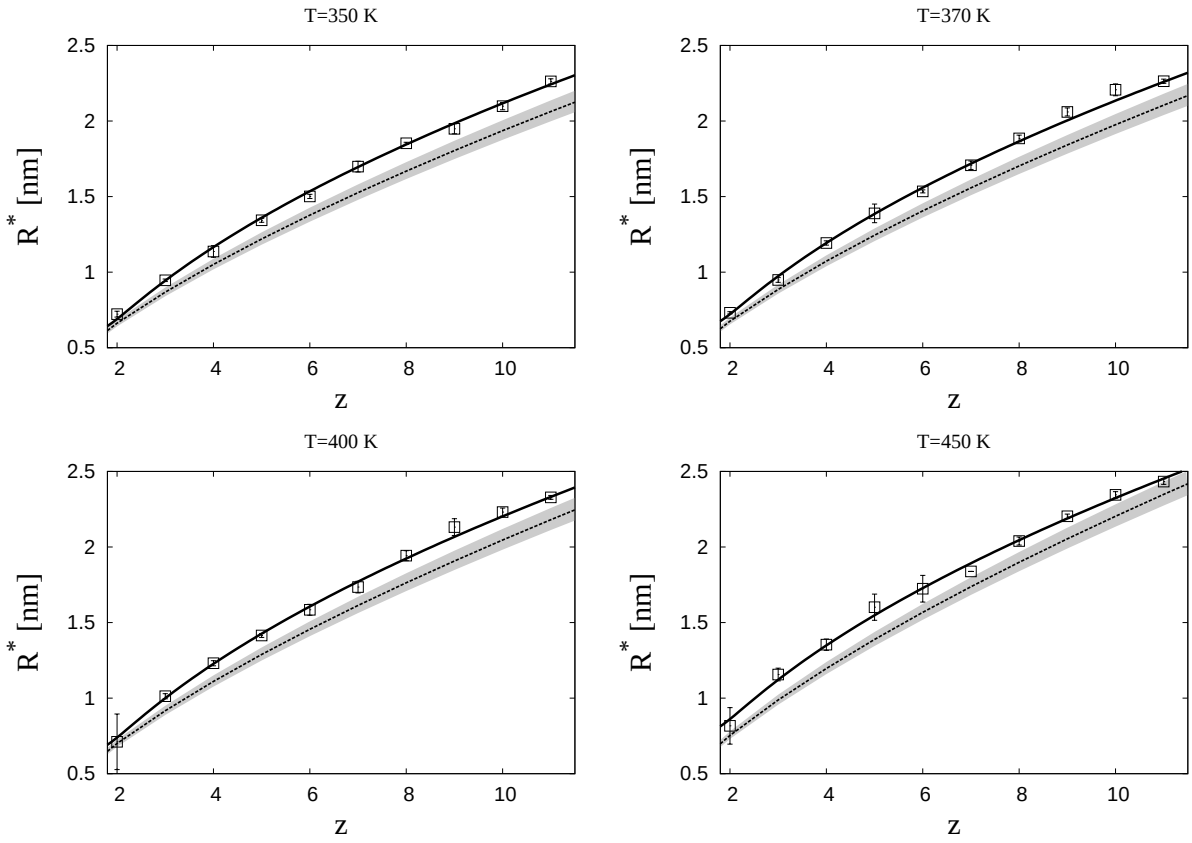

FIG. 3: The critical radius $R^*(z)$ at $T = 350, 370, 400$, and 450 K. The squares represent the averaged data for different simulation runs and the error bars the standard deviation. Dashed and solid lines correspond to Rayleigh theory given be Eq. (2) and the least-squares fitting of the simulation data, respectively. The gray region around the Rayleigh theory shows the uncertainty that arises from the $\pm 10\%$ variation in the surface tension.

for droplets containing a larger number of charges. This increase relative to their size is from 30% to 15% , respectively. Such difference in the number of molecules in the main droplet leads to a large difference in the activation energy, as extracted from the reversible work profiles in Ref. 13 , and therefore results in large difference in the fragmentation rate. An example is presented in Ref. 13, where the reversible work profiles and the fragmentation rate were estimated for systems that consist of 4 Cl^- and 170-220 H_2O molecules at $T = 250$ K. The barrier height in the reversible work profiles changes from $3.5k_BT$ for 170 H_2O molecules to $10k_BT$ for 220 H_2O molecules. Between 190-210 H_2O molecules the barrier is approximately $6k_BT$ and with the dynamic corrections results to inverse nanosecond time scale for the rate of fragmentation. In Table I, the case of 4 Cl^- is also included for $T = 350$ to 450 K and is found that the vast majority of fissions for these systems occur between 170-220 water molecules. There are also few fragmentations that occur when the number of water molecules in the droplet is 150-166. Studies in Ref. 13 suggest that break down with a a free energy barrier less than $3.5k_BT$ will occur when the number of water molecules is below 170. This lower limit of approximately 170 H_2O molecules will be increased slightly for the higher temperatures studied here. For the fragmentation of clusters with sizes between 150-166 water molecules there are two possible scenarios: i) they may break down spontaneously by any small shape fluctuation and not by specific rare fluctuations that give rise to a free energy barrier at the breaking point; ii) an ion-evaporation type of mechanism may continue to exist where only a "late" transition state appears few Angstroms away from the surface of the mother droplet as is described in Ref. 19. The possibility of these two mechanisms need further investigation.

Our findings are in agreement with the results in Ref. 19 where in the case of water the proximity of the ion evaporation line and the Rayleigh line was noted as well as larger differences for other solvents.

The picture that emerges from the simulations about the mechanism and the validity of Rayleigh's theory for nanodrops is the following: For this particular system Rayleigh's model provides a good energetic criterion for spontaneous break down. When the system approaches this criterion, close to one solvation shell beyond that R_R predicts, it may break down by an activated process. Since there is a distribution in the sizes of droplets that contain a certain amount of charge, the mechanism

will be a mixture of fragmentations that are activated processes for the majority of the droplets with possible spontaneous Rayleigh-type fragmentations for the smallest droplets. For the smallest sizes of systems the type of mechanism, Rayleigh micro-explosion or ion-evaporation need to be investigated. However, a Rayleigh micro-explosion is more likely because the dominant Coulomb repulsion among the ions will accelerate the solvated ion when it breaks from the mother droplet and the adjustment of the polarization that will prevent the escape in a late transition state will not have time to be established.

C. IEM models

1. *Born Theory and simulations*

While Rayleigh's theory yields the critical radius for the energetic break down of a charged drop due to critical fluctuations, Born's model deals with the energetic outcome of the break down and is often used as a basic component of models for IEM.[7] In Born's model the thermodynamic reversible work to move a cluster with radius R_d containing a solvated ion from uncharged liquid with flat surface to vacuum is equal to the Gibbs free energy, and is given by

$$\Delta^\circ = \frac{e^2}{8\pi\epsilon_0 R_d} + 4\pi\gamma R_d^2. \tag{4}$$

In Eq. (4) the term $O(1/\epsilon)$ is neglected for a solvent with a relative dielectric constant ϵ that is much greater than unity. The free energy Δ° is a function of R_d with minimum value

$$\Delta G_S^\circ := \Delta^\circ(R_B) = \frac{3}{4\pi^{1/3}} \frac{e^{4/3}\gamma^{1/3}}{\epsilon_0^{2/3}}, \tag{5}$$

which is attained at the Born radius, R_B, given by

$$R_B = \left(\frac{e^2}{64\pi^2\epsilon_0\gamma}\right)^{1/3}. \tag{6}$$

Before comparing the simulation results with R_B, let us examine the effect of the main droplet's charge z on R_d. Here we focus only on the daughter droplets with a single ion since those with more than a single ion scarcely appear. Figure 4 shows the variations of R_d with the charge of the main droplet at $T = 350$ K. The data do not show any systematic dependence of R_d on z, while in that range of z, the size of the main droplet R changes more than twice. For other temperatures, the results are similar. Thus, we conclude that R_d does not depend on z for the sizes of systems examined here.

In Fig. 5, the Born radius R_B and simulation results of R_d for single-ion daughter droplets versus temperature T are shown. R_d is larger than R_B by 0.1 to 0.15 nm. The standard deviations of R_d, 0.064, 0.048, 0.059, and 0.076 nm at $T = 350, 370, 400$, and 450 K respectively,

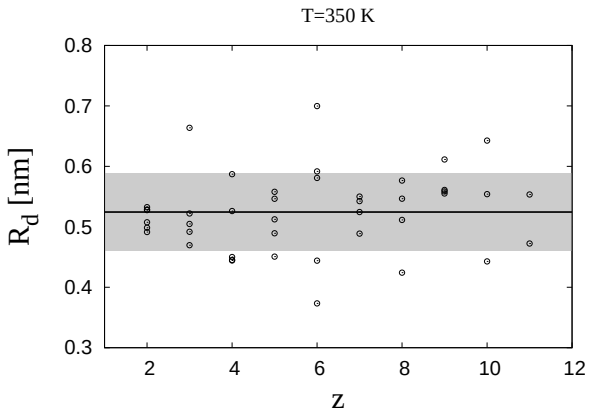

FIG. 4: R_d versus charge z of the parent droplet at $T = 350$ K. The solid line and gray region show the average (0.52 nm) and the standard deviation ($\pm$0.064 nm) of the present data, respectively.

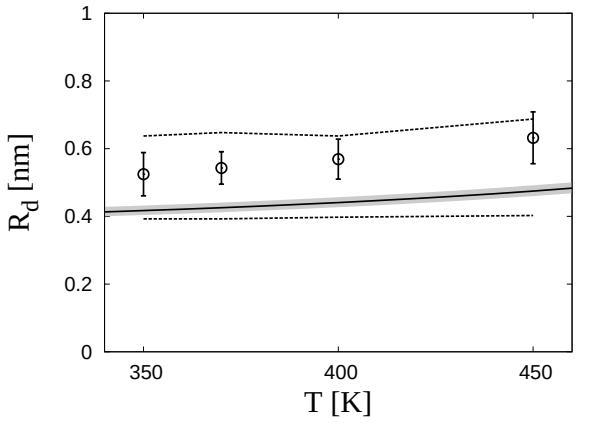

FIG. 5: Radius of the daughter droplets, R_d, with $z = 1$. The open circles correspond to the mean values and the error bars show the standard deviations. The lower and upper dashed lines mark the boundaries of the first and second solvation shells around Cl^-. The solid line is R_B surrounded by a gray region that shows the uncertainty in the estimation of R_B that arises from $\pm$10% variation in the surface tension.

are relatively large. However, they are of similar size as for R^*, which are 0.024, 0.029, 0.073, and 0.067 nm, respectively. Since we have typically only three independent events for each set of parameters (z, T), the above dispersion is reasonable.

a. The journey of the ion To interpret the results, it is useful to look initially into the solvation state of the ion in the main droplet. The radial distribution function $g(r)$ between the chloride and oxygen atomic sites in the main droplet are evaluated for each run from the beginning to the time before the charge in the main droplet becomes unity for three simulations starting from $N = 1600$ and $z = 11$ at each temperature. It is found that the first solvation shell may extend up to 0.4 nm and the second solvation shell may extend to 0.64$-$0.65 nm at $T = 350-400$

K and 0.69 nm at $T = 450$ K. These boundaries are also shown by dashed lines in Fig. 5. We also estimate the

T [K]	N_d	N_h^1	N_h^2
350	18 ± 8.3	7.32	22.6
370	19 ± 5.5	7.28	23.4
400	22 ± 7.2	7.34	20.9
450	30 ± 8.7	7.26	24.0

TABLE II: N_d with its standard deviation, and the hydration numbers of the first and second solvation shells of Cl^-, N_h^1 and N_h^2, respectively.

average number of water molecules N_d in the daughter droplets as well as the hydration numbers N_h^1 and N_h^2 of the first and second solvation shells of Cl^-, respectively (Table II). The values of N_h^1 are close to 7.4 as for the hydration number of bulk water at $T = 298$ K obtained by MD simulations with the same SPC/E model and ion parameters.[23] Furthermore, the position of the first peak and first minimum in $g(r)$ are also close to the bulk values found at 0.32 and 0.40 nm, respectively.

To look into more detail in the solvation of the ions in the course of the fragmentations, we present the picture from a typical realization at $T = 370$ K starting from $N = 1600$ and $z = 11$. Instead of integrating $g(r)$, we use two spherical regions around each ion to characterize the ion solvation state. These spheres correspond to the first and second solvation shells, with radii at 0.40 nm and 0.64 nm, respectively taken from the $g(r)$. Figure 6

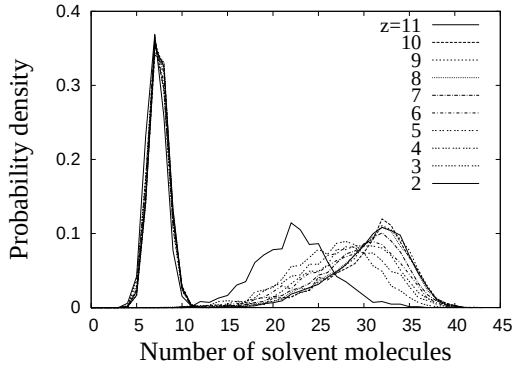

FIG. 6: Probability densities of N_h^1 and N_h^2, the numbers of solvent molecules in the spherical regions around the ion with radii 0.40 nm (left sharp peaks) and 0.64 nm (right broader peaks), for each duration of z for a typical realization at $T = 370$ K.

shows the probability densities of N_h^1 and N_h^2, the numbers of solvent molecules in those spherical regions, for the duration between each fragmentation event (characterized by z in fig. 6). The sharp and stable peaks around 7 correspond to N_h^1 and the broader peaks to N_h^2. The structure of the first solvation shell is quite stable in the course of the fragmentation events as indicated by the first peak in fig. 6. This concludes that the ions in the main droplet are found at least one solvation shell below the surface rather than exposed on the surface. On the other hand, the peak of the second solvation shell shifts gradually as N and z decrease. This shift will be due to the change in the droplet size than in the number of charges.

This result is different from previous findings that a single Cl^- in a small water cluster prefers surface solvation.[37,41–43] This might be due to use of non-polarizable model in the present simulations while a polarizable model is necessary to reproduce the behavior by MD simulations.[37,41] However, the difference of the situations should also be noted; the present system has many ions in a cluster, while the above results[37,41–43] are for a single ion in a cluster.

When the solvated ion detaches, for temperatures as low as $T = 350$ K, there are a few daughter droplets which leave with the fist solvation shell surrounding the Cl^-, while the majority of the droplets leave with their second solvation shell partially filled. The higher the temperature the more water molecules are contained in the daughter droplets, and more short open chain structures than closed compact structures of water around Cl^- are favored. As a result, the higher the temperature the radius appears to be larger. The Born radius coincides with the boundaries of the first solvation shell of Cl^- for $T = 350 - 400$ K. The difference between the simulation data and Born's theory can be explained in the following way: The number of water molecules that the daughter droplet will carry depends largely on the process that occurs at the barrier top of the activated process, while Born's theory only takes into account the initial and final states. An example of this scenario is shown in Fig. 2. Configurations (a) and (c) correspond to the barrier top of the activated process as described in Refs. 12,13. The departing solvated ion may return to the main droplet as in Fig. 2 (b), or it may leave the main droplet, pinching at certain point in the bridge as in Fig. 2 (d). The resultant daughter droplet, therefore, consists of the ion with at least its first solvation shell and a portion of the water molecules from the bridge structure.

2. Ion Evaporation Models

Iribarne and Thomson[7] used the Born theory to construct an ion evaporation model for the generation of gas-phase ions in electrospray. In IEM a small cluster that contains the ion and several solvent molecules is evaporated from the main droplet by an activated process that follows first-order reaction kinetics. The original IEM model was extended by Fernández de la Mora *et al.* by taking into account the dielectric medium[8,44] and curvature effects.[19,40] The activation energy, Δ, was expressed as[19]

$$\Delta = \Delta^\circ - \frac{e^2}{8\pi\epsilon_0 R}\Big\{1 + 2F(z-1)\Big\} - \frac{8\pi\gamma R_d^3}{3R}, \qquad (7)$$

where, in the right-hand side, Δ° is given by Eq. (4), the second term is the charge correction and the third term is the curvature correction. The function $F(z)$ is a known function coming from the maximization of the electrostatic energy of two conducting spheres. The numerical form of $F(z)$ is given up to $z = 10$ in Ref. 8 and up to $z = 20$ in Appendix B. In Eq. (7) the terms of order $O(1/\epsilon)$ and $O(R_d^3/R^3)$ are neglected.

If the ion fragmentation for the droplet with z ions occurs at the critical size R^*, the activation energy of the fragmentation process is given by $\Delta^* = \Delta(R^*, z)$. As in Refs. 40,45, we will try to fit the charge-dependence of the critical radius $R^*(z)$ by

$$R^*(z) = \Gamma\Big\{F(z-1) + \alpha\Big\}. \tag{8}$$

Γ and α are related to the physical quantities by

$$\Gamma = \frac{4R_B}{\frac{2}{x} + x^2 - \frac{3\Delta^*}{\Delta G_S^\circ}}, \tag{9}$$

$$\alpha = \frac{1}{2} + \frac{x^3}{6}, \tag{10}$$

where $x = R_d/R_B$ and R_B and ΔG_S° are given by Eqs. (6) and (5), respectively. Using the simulation data, the

T [K]	α	Γ [nm]
350	0.326	0.811
370	0.374	0.803
400	0.364	0.832
450	0.541	0.827

TABLE III: Fitting results of Eq. (8) for $R^*(z)$ by the extended IEM model. The parameters are obtained for the entire range of z.

parameters Γ and α are found by the least-squares fitting of R^*, and the results are summarized in Table III. The fitting represents the behavior of $R^*(z)$ as shown in Fig. 3. However, from Eq. (10), it is expected that $\alpha > 1/2$ while most of the results are with $\alpha < 1/2$. Because the assumptions of $R \gg R_d$ made in the derivation of Eq. (7) is marginal in the present case, we left α in Eq. (8) as an unknown curvature parameter as in the literature.[40,45] The activation energy Δ^* is found from Eq. (9), and the characteristic time τ is then estimated from

$$\tau = \frac{h}{k_B T} \exp\left(\frac{\Delta^*}{k_B T}\right), \tag{11}$$

where h is the Planck constant. Instead of minimizing Δ to determine R_d, there are two possible choices for x in the model: $x = R_d/R_B \approx 1.3$ from the simulations, or $x = 1$ from the assumption of $R_d = R_B$. For the two cases, the estimations of Δ^* and τ are summarized in Table IV. It is clear that the activation energies for both cases are rather high and the characteristic time too long. Since Δ^* can be written as

$$\Delta^* = \Delta^\circ(R_d) - \frac{e^2}{4\pi\epsilon_0\Gamma}, \tag{12}$$

	$x = R_d/R_B$		$x = 1$		
T [K]	Δ^* [eV]	τ [s]	Δ^* [eV]	τ [s]	ΔG_S° [eV]
350	0.96	9.5	0.81	7.0×10^{-2}	0.757
370	0.91	3.1×10^{-1}	0.74	1.7×10^{-3}	0.772
400	0.89	2.2×10^{-2}	0.72	1.3×10^{-4}	0.793
450	0.74	2.1×10^{-5}	0.53	9.9×10^{-8}	0.839

TABLE IV: Activation energy Δ^* and characteristic time τ estimated from Γ. The second column is obtained with $x = R_d/R_B$ while the third with $x = 1$. ΔG_S° is given by Eq. (5).

where Γ is used as an unknown parameter given from the fitting in Eq. (8), the possible cause of the high activation energy is Δ°. In the case of $R_d = R_B$, Δ° reduces to ΔG_S°, which is also shown in Table IV and actually this estimation from the Born theory is higher than the solvation energy for Cl^-. This point as well as the unknown curvature parameter α need to be established to complete the picture of the ion evaporation model.

Since the dynamics of the present simulations is not real but canonical dynamics, another approach for activated processes as presented in Refs. 12,13 may be used to compute the rate of ion evaporation. If the rate is available one can find the thermodynamic activation energy and compare with the various IEM models.

IV. CONCLUSIONS

In terms of constant-temperature molecular dynamics simulations, the mechanism of ion fragmentation of charged aqueous nanodroplets composed of water molecules and chlorine ions was examined. In contrast to previous simulation studies, the solvent evaporation is taken into account directly and sequences of fragmentation events are observed. The droplets give birth mainly to solvated single ions and to only very few daughter droplets with two ions with several solvent molecules. In the simulations the size of the critical radius $R^*(z)$ and that of the daughter droplets R_d, are estimated directly. It is found that the agreement in $R^*(z)$ between Rayleigh's model and simulations is within 0.23 nm or in terms of charge is 87%. However, the small difference in radius is caused by a large number of water molecules that may give rise to an activated process that follows first-order reaction kinetics as described in Refs. 12,13.

From the present data, the picture that emerges for the fragmentation mechanism is as follows: The droplet shrinks by evaporation till it reaches a certain size. This size can be described in a macroscopic way by an average critical radius or at the molecular level by a distribution in the number of water molecules that the main droplet contains. The number of water molecules can change the barrier of the reversible work profiles and, therefore the fragmentation rate. Fragmentation happens through fluctuations where a solvated ion protrudes considerably from the bulk of the droplet and is connected to it by a

bridge of water molecules. In the language of activated processes thorned or bridged configurations correspond to the barrier of the reversible work profile as presented in 12,13.

The size of the daughter droplet R_d given by the Born model is smaller by 0.1 to 0.15 nm than the simulation findings. The size distribution of the daughter droplets depends on the dynamics of the configurations at the barrier top of a reversible work profile for the activated process, which is missing in Born's theory. The formation of water bridges close to fragmentation affects the number of water molecules that the daughter droplets may carry. Application of an extended IEM model to $R^*(z)$ yields very large time scales for the fragmentation of nanodrops. This suggest that a direct use of the same model in nanodrops is weak and improvement on the parameters is required.

A number of open questions still exist: Under what conditions one may observe Rayleigh micro-explosion and how the fragmentation mechanism changes by the type of interactions and temperature? More detailed investigation of the assumptions of IEM and the nature of the transition state (TS) are required. IEM models assume a late TS where the two droplets are already separated and macroscopically are subjected to electrostatic repulsion due to their similar charge and electrostatic attraction due to their polarization. However, the microscopic picture from the present simulations and Refs. 12,13 suggest that there is an ensemble of configurations that correspond to a TS where the departing ion is strongly connected to the remaining droplet. Simulations in Refs. 12,13 find a free energy barrier at the breaking point[4] that leads to nanosecond time scale for ion evaporation. Investigation of a possible free energy barrier after the detachment of the ion is needed. The interplay between the time required to establish a late barrier due to the adjustment of the polarization of the mother and daughter droplets and the speed that the ion leaves is an interesting question. Currently, we study the fragmentation for droplets larger than the droplets described in this study and address the above questions.

Acknowledgments

SC thanks the Natural Sciences and Engineering Research Council of Canada (NSERC) for funding this research and NSERC and Canada Foundation for Innovation (CFI) for a grant that allowed us to have the computing facilities used for the computations in this project. SC thanks Prof. Dr. E. W. Schlag in the Technical University of Munich for stimulating discussions on Rayleigh's model. The authors thank Professor Lars Konermann and Minh Trang Tran for helpful discussions, and Kirkland R. Mainer for useful comments on the manuscript.

APPENDIX A: ESTIMATION OF THE CLUSTER RADIUS

To characterize functions of macromolecules such as protein and nucleic acids, three types of molecular surface models – the solvent-accessible (SA) surface, molecular surface (MS) and van der Waals (VDW) surface – have been developed.[29] The VDW surface of a group of atoms consists of the spheres whose radius is the van der Waals radius of the atoms. If two spheres overlap, only the exposed portion of the spheres is taken as the surface. For the MS and SA surfaces, a probe particle is introduced, which represents a solvent molecule used to determine the reaction surface between the macromolecule and the solvent. The SA surface is the trace of the probe center when it moves all over the VDW surface. Therefore, the SA surface is always placed outside the VDW surface by the probe radius R_p. The MS surface, on the other hand, is the collection of the most inner points of the probe surface over the VDW surface. That is, it consists of the VDW surface when the probe contacts only one point and the reentrant surface which is a part of the probe surface when the probe contacts two or more points.

To determine which model is suitable for calculating the radius of droplets in the present case, we prepared perfect spherical droplets extracted from bulk configurations. Two configurations were used to test the surface models: (a) a spherical configuration that is specified by the number of atoms and (b) a spherical configuration that is specified by the radius of the spherical region. Configuration (a) consists of 1600 water molecules and 11 ions and the distance between the origin and the center of the most outer oxygen site is $R_0 = 2.256$ nm. This distance is a reference number for the cluster radius estimation using the various surface models. Configuration (b) contains 1097 water molecules and all oxygen centers of the water molecules are in a spherical region with reference radius $R_0 = 2.0$ nm. For these configurations, the volume of the cluster, V, was calculated for the VDW, MS and SA models and the radius $R = (3V/4\pi)^{1/3}$ was estimated. Since the SA model has a layer with thickness R_p outside the VDW surface, we also estimated the radius $R_{SAP} = R_{SA} - R_p$. Therefore, we tested the four estimations of radii. The results for the two configurations are summarized in Table V. As expected from the construction of the models, the radius of VDW is the smallest and that of SA is the largest. Compared to the reference value R_0, for both configurations, the SAP estimation is the best. Therefore, the SA model with subtraction of the probe radius would be used for the estimations of the radius of a cluster.

APPENDIX B: FUNCTION $F(z)$

The function $F(z)$ in Eq. (7) is defined in Ref. 8 by

$$F(z) = z - f(x^*(z)), \tag{B1}$$

config.	R_0 [nm]	model	R [nm]	$R - R_0$ [nm]
(a)	2.256	VDW	1.876	-0.380
		MS	2.219	-0.037
		SAP	2.271	+0.015
		SA	2.411	+0.155
(b)	2.0	VDW	1.650	-0.350
		MS	1.940	-0.060
		SAP	1.998	-0.002
		SA	2.138	+0.138

TABLE V: Radii for configurations (a) and (b) using VDW, MS, SA and SAP models.

where $f(x)$ is given by

$$f(x) := \frac{z}{x} - \frac{1}{2x^2(x^2-1)}, \tag{B2}$$

and $x^*(z)$ is the value where f has its maximum. From $\mathrm{d}f/\mathrm{d}x = 0$, we get

$$z = \frac{2x^2-1}{x(x^2-1)^2}. \tag{B3}$$

Solving B3 for integer values of z, we get $x^*(z)$, which is found by a simple numerical root-finding code. In Ref. 8, $F(z)$ is tabulated up to $z = 10$. For reference purposes,

z	$x^*(z)$	$F(z)$
1	1.6180340	0.5000000
2	1.4275639	0.8353900
3	1.3433693	1.1111408
4	1.2936254	1.3515610
5	1.2599984	1.5677242
6	1.2353957	1.7658505
7	1.2164289	1.9498640
8	1.2012521	2.1224348
9	1.1887646	2.2854796
10	1.1782644	2.4404306
11	1.1692807	2.5883921
12	1.1614846	2.7302369
13	1.1546386	2.8666695
14	1.1485663	2.9982683
15	1.1431339	3.1255151
16	1.1382375	3.2488166
17	1.1337954	3.3685195
18	1.1297423	3.4849225
19	1.1260252	3.5982850
20	1.1226005	3.7088341

TABLE VI: Numerical results of $x^*(z)$ and $F(z)$.

the results are presented in Table VI up to $z = 20$ in single precision accuracy while the calculation is done in double precision.

* Electronic address: sconstas@uwo.ca

[1] Rayleigh, L. *Phil. Mag.* **1882**, *14*, 184–186.

[2] Cole, R. B., Ed.; Wiley-Interscience: New York, 1997.
[3] Fenn, J. B.; Mann, M.; Meng, C. K.; Wong, S. F.; Whitehouse, C. M. *Science* **1989**, *246*, 64–71.
[4] Kebarle, P. *J. Mass Spectrom.* **2000**, *35*, 804–817.
[5] Fenn, J. B. *Angew. Chem. Int. Ed.* **2003**, *42*, 3871–3894.
[6] Dole, M.; Mack, L. L.; Hines, R. L.; Mobley, R. C.; Ferguson, L. D.; Alice, M. B. *J. Chem. Phys.* **1968**, *49*, 2240–2249.
[7] Iribarne, J. V.; Thomson, B. A. *J. Chem. Phys.* **1976**, *64*, 2287–2294.
[8] Gamero-Castaño, M.; Fernández de la Mora, J. *Anal. Chim. Acta* **2000**, *406*, 67–91.
[9] Fenn, J. B.; Rosell, J.; Nohmi, T.; Shen, S.; F. J. Banks, J. In *Biochemical and Biotechnological Applications of Electrospray Ionization Mass Spectrometry*; Snyder, A. P., Ed.; American Chemical Society: Washington, D.C., 1996.
[10] Kebarle, P.; Peschke, M. *Anal. Chim. Acta* **2000**, *406*, 11–35.
[11] Gabelica, V.; De Pauw, E. *Mass Spectrometry Reviews* **2005**, *24*, 566–587.
[12] Consta, S. *J. Mol. Structure (Theochem)* **2002**, *591*, 131–140.
[13] Consta, S.; Mainer, K. R.; Novak, W. *J. Chem. Phys.* **2003**, *119*, 10125–10132.
[14] Znamenskiy, V.; Marginean, I.; Vertes, A. *J. Phys. Chem. A* **2003**, *107*, 7406–7412.
[15] Marginean, I.; Znamenskiy, V.; Vertes, A. *J. Phys. Chem. B* **2006**, *110*, 6397–6404.
[16] Last, I.; Levy, Y.; Jortner, J. *Proc. Natl. Acad. Sci. U.S.A.* **2002**, *99*, 9107–9112.
[17] Last, I.; Levy, Y.; Jortner, J. *J. Chem. Phys.* **2005**, *123*, 154301.
[18] Levy, Y.; Last, I.; Jortner, J. *Mol. Phys.* **2006**, *104*, 1227–1237.
[19] Labowsky, M.; Fenn, J. B.; Fernández de la Mora, J. *Anal. Chim. Acta* **2000**, *406*, 105–118.
[20] Basaran, O. A.; Scriven, L. E. *Phys. Fluids A* **1989**, *1*, 799–809.
[21] Berendsen, H. J. C.; Grigera, J. R.; Staatsma, T. P. *J. Phys. Chem.* **1987**, *91*, 6269.
[22] Chandrasekhar, J.; Spellmeyer, D. C.; Jorgensen, W. L. *J. Am. Chem. Soc.* **1984**, *106*, 903–910.
[23] Balbuena, P. B.; Johnston, K. P.; Rossky, P. J. *J. Phys. Chem.* **1996**, *100*, 2706–2715.
[24] van der Spoel, D.; Lindahl, E.; Hess, B.; Groenhof, G.; Mark, A. E.; Berendsen, H. J. C. *J. Comp. Chem.* **2005**, *26*, 1701–1718.
[25] Hockney, R. W.; Goel, S. P. *J. Comp. Phys.* **1974**, *14*, 148.
[26] Berendsen, H. J. C.; Postma, J. P. M.; DiNola, A.; Haak, J. R. *J. Chem. Phys.* **1984**, *81*, 3684–3690.
[27] Hoover, W. G. *Phys. Rev. A* **1985**, *31*, 1695–1697.
[28] Nosé, S. *Mol. Phys.* **1984**, *52*, 255–268.
[29] Richards, F. M. *Annu. Rev. Biophys. Bioeng.* **1977**, *6*, 151–176.
[30] Connolly, M. L. *J. Appl. Crystography* **1983**, *16*, 548–558.
[31] Connolly, M. L. *J. Am. Chem. Soc.* **1985**, *16*, 1118–1124.
[32] Ponder, J. W. http://dasher.wustl.edu/tinker/.
[33] IAPWS. *IAPWS Release on Surface Tension of Ordinary Water Substance* **1994**.
[34] Tolman, R. C. *J. Chem. Phys.* **1949**, *17*, 333–337.
[35] van Giessen, A. E.; Blokhuis, E. M. *J. Chem. Phys.* **2002**, *116*, 302–310.
[36] *Current Opinion Colloids Interface Sci.* **2004**, *9*, 1–197.
[37] Jungwirth, P.; Tobias, D. J. *Chem. Rev.* **2006**, *106*, 1259–1281.
[38] Weissenborn, P. K.; Pugh, R. J. *J. Colloid Interface Sci.* **1996**, *184*, 550–563.
[39] Smith, J. N.; Flagan, R. C.; Beauchamp, J. L. *J. Phys. Chem. A* **2002**, *106*, 9957–9967.
[40] Gamero-Castaño, M.; Fernández de la Mora, J. *J. Mss Spectrom.* **2000**, *35*, 790–803.
[41] Perera, L.; Berkowitz, M. L. *J. Chem. Phys.* **1991**, *95*, 1954–1963.
[42] Combariza, J. E.; Kestner, N. R.; Jortner, J. *J. Chem. Phys.* **1994**, *100*, 2851–2864.
[43] Markovich, G.; Pollack, S.; Giniger, R.; Cheshnovsky, O. *J. Chem. Phys.* **1994**, *101*, 9344–9353.
[44] Loscertales, I. G.; Fernández de la Mora, J. *J. Chem. Phys.* **1995**, *103*, 5041–5060.
[45] Ku, B. K.; Fernández de la Mora, J. *J. Phys. Chem. B* **2005**, *109*, 11173–11179.